Article:
Wang, N., Robaye, B., Agrawal, A. et al. (2011) Reduced Bone Turnover in Mice Lacking the P2Y13 Receptor of ADP. Molecular Endocrinology, 26 (1). pp. 142-152. ISSN: 0888-8809

https://doi.org/10.1210/me.2011-1083

Title: Reduced bone turnover in mice lacking the $P2Y_{13}$ receptor of ADP.

Short Title: Reduced bone turnover in $P2Y_{13}$ KO mice

Ning Wang[a], Bernard Robaye[b], Ankita Agrawal[a], Timothy M. Skerry[a], Jean-Marie Boeynaems[b,c], Alison Gartland[a1]

[a]The Mellanby Centre for Bone Research, Department of Human Metabolism, The University of Sheffield, Sheffield, UK, [b]Institute of Interdiscipinary Research, IRIBHM, Université Libre de Bruxelles, Gosselies, Belgium, [c] Department of Medical Chemistry, Erasme Hospital, Brussels, Belgium

1 Corresponding author and person to whom reprint requests should be addressed:

Dr Alison Gartland,

The Mellanby Centre for Bone Research

Department of Human Metabolism

The University of Sheffield

Beech Hill Road

Sheffield, S10 2RX

UK

Phone: (+44) 0114 226 1435

Fax: (+44) 0114 271 1711

Email: a.gartland@sheffield.ac.uk

Key words: $P2Y_{13}$ receptor, knock-out, osteoblasts, osteoclasts, OVX

Funding Source: European Commission under the 7th Framework Programme (proposal #202231) performed as a collaborative project among the members of the ATPBone Consortium (Copenhagen University, University College London, University of Maastricht, University of Ferrara, University of Liverpool, University of Sheffield, and Université Libre de Bruxelles), and is a sub study under the main study "Fighting osteoporosis by blocking nucleotides: purinergic signalling in bone formation and homeostasis"

Disclosure summary:

All authors have nothing to disclose.

Abstract:

Osteoporosis is a condition of excessive and un-coupled bone turnover in which osteoclastic resorption exceeds osteoblastic bone formation, resulting in an overall net bone loss, bone fragility and morbidity. While numerous treatments have been developed to inhibit bone loss by blocking osteoclastic bone resorption, understanding of the mechanisms behind bone loss is incomplete. The purinergic signalling system is emerging to be a pivotal regulator of bone homeostasis and extracellular ADP has previously been shown to be a powerful osteolytic agent in vitro. We report here that deletion of the $P2Y_{13}$ receptor, a G-protein coupled receptor for extracellular ADP, leads to a 40% reduction in trabecular bone mass, 50% reduction in osteoblast and osteoclast numbers in vivo as well as activity in vitro and an overall 50% reduction in the rate of bone remodelling in mice in vivo. Down-regulation of RhoA/ROCK I signalling and a reduced ratio of RANKL/OPG observed in osteoblasts from $P2Y_{13}R^{-/-}$ mice might explain this bone phenotype. Furthermore, as one of the main causes of osteoporosis in older women is lack of estrogen, we examined the effect of ovariectomy (OVX) of the $P2Y_{13}R^{-/-}$ mice and found them to be protected from OVX-induced bone loss by up to 65%. These data confirm a role of purinergic ADP signalling in the skeleton, whereby deletion of the receptor leads to reduced bone turnover rates which provide a protective advantage in conditions of accelerated bone turnover such as oestrogen deficiency-induced osteoporosis.

Key words: $P2Y_{13}$ receptor, knock-out, osteoblasts, osteoclasts, OVX

Introduction

The membrane-bound receptors for extracellular nucleotides known as P2 receptors can be divided into two major families based on their signal transduction mechanisms and topology. P2X receptors form a family of ligand-gated ion channels with signal transduction cascade via non-selective outward cation currents, whilst P2Y receptors form a family of G protein-coupled receptors coupled to G_q or/and G_i (1). Both osteoblasts and osteoclasts express numerous P2 receptor subtypes in a spatial and temporal manner (2). Specifically in osteoblasts, ATP and its degradation product adenine diphosphate (ADP) have been shown to modulate $[Ca^{2+}]_i$ calcium signalling (3), increase cell proliferation (4), increase expression of Receptor Activator of NF-κb Ligand (RANKL) (a key modulator of osteoclast formation and resorption) (5) and intriguingly, synergise with PTH to induce activation of c-*fos*, a key transcription factor in bone (6). This last observation suggests that ATP and P2 receptors represent a local mechanism enabling the bone remodelling induced by systemic hormones such as PTH to be confined to discrete foci. In osteoclasts, ATP appears to have both stimulatory (7, 8) and inhibitory roles via P2 receptors (9, 10), whilst ADP was shown to be a powerful osteolytic agent reportedly acting via the $P2Y_1$ receptor (11). *In vivo* knockout models have offered further insights into the overall effect on bone homeostasis of the different, but highly significant effects of extracellular nucleotides. $P2Y_2$ receptor deficient mice demonstrate a striking increase in bone mineral content, presumably related to the inhibitory effect of ATP on mineralization by osteoblasts (12). On the contrary, the $P2X_7$ receptor deficient mice do not have an extreme skeletal phenotype (13) but exhibit site-specific alterations in bone formation and resorption (14). A recent preliminary investigation of $P2Y_1$ receptor deficient mice revealed a reduced bone mass, confirming a role for ADP in bone homeostasis (15).

In addition to the $P2Y_1$ and $P2Y_{12}$ receptor, the $P2Y_{13}$ receptor, originally named GPR86 (16), has high affinity for ADP (17). The $P2Y_{13}$ receptor is a G_i-coupled receptor which shows a high level of identity with $P2Y_{12}$ and $P2Y_{14}$ receptors, sharing 45-48% amino acid sequence identity (17). Similarly to the $P2Y_1$ and $P2Y_{12}$ receptors, $P2Y_{13}$ receptors respond to ADP in the nanomolar range (18). Expression of $P2Y_{13}$ receptor mRNA has been shown in abundance in the brain, spleen, lymph nodes

and bone marrow, suggesting roles in nervous, haematopoietic, and immune systems. A lower level of expression is found in liver, lung, placenta, and spinal cord (17-19). Although $P2Y_{13}$ receptors are detected in different tissues, the physiological function of this receptor is still unclear. Several reports suggesting a role of $P2Y_{13}$ receptors are not entirely convincing due to the lack of truly selective agonists and antagonists for this receptor (20-25). Indeed Cangrelor (AR-C69931MX) behaves as a $P2Y_{13}$ receptor antagonist (26) or partial agonist (27), although it was primarily described as a specific $P2Y_{12}$ receptor antagonist and is currently in clinical development as an antithrombotic agent. The study of $P2Y_{13}$ receptor-deficient mice ($P2Y_{13}R^{-/-}$) has so far revealed the role of this receptor in HDL cholesterol uptake by hepatocytes and reverse cholesterol transport (28, 29). In the context of bone, the expression of $P2Y_{13}$ receptors in osteoblasts and osteoclasts has been recently confirmed (30, 31). Taken together with the previous reports of the powerful effect of ADP on osteoclasts, we sought to determine the consequence of $P2Y_{13}$ receptor gene deletion on the bones of mice. Using micro computer tomography (μCT) we show that the bones of the $P2Y_{13}R^{-/-}$ mice have altered bone mass, due to reduced numbers of osteoblasts and osteoclasts in the bone as shown by histology. Dynamic histomorphometry confirmed reduced mineral apposition and bone formation rates, whilst *in vitro* primary cell cultures were used to determine the effect of gene deletion on the formation and function of osteoblasts and osteoclasts. Finally, ovariectomy (OVX), a widely accepted model of bone changes after menopause (32), revealed that $P2Y_{13}R^{-/-}$ mice were protected from OVX-induced bone loss by up to 65%. These findings confirm a role for the $P2Y_{13}$ receptor in bone remodelling, offering a potential novel therapeutic target for fighting bone diseases in conditions of accelerated bone turnover such as oestrogen deficiency-induced osteoporosis.

Results

Reduced trabecular bone volume in $P2Y_{13}R^{-/-}$ mice

There was no severe or obvious gross morphological difference between the whole skeleton of $P2Y_{13}R^{-/-}$ and wild type (WT) mice upon macroscopic examination or using μCT 3D models of the whole tibia (Fig. 1*A*). However, μCT analysis revealed that although the length of the tibia was not significantly different, $P2Y_{13}R^{-/-}$ mice had ~5% less total bone volume in the tibia compared with WT

(Fig. 1C, $p < 0.05$). Analysis of the microstructure of the bone in the tibia at a higher resolution revealed 37.5% less trabecular bone ($p < 0.001$)(Fig. 1*D*) and 37.8% fewer trabeculae in $P2Y_{13}R^{-/-}$ mice compared to WT ($p < 0.001$) (Fig. 1*E)*. Other typical trabecular bone parameters are summarised in Table 1. μCT analysis on a predominantly cortical bone region showed no significant effects on cortical bone parameters including cortical bone volume ($p = 0.09$), endosteal diameter ($p = 0.41$) and periosteal diameter ($p = 0.48$) (Table 1).

Reduced osteoclast and osteoblast numbers in long bones of $P2Y_{13}R^{-/-}$ mice

Assessment of the cellular compartment of the bone by histological analysis showed that there were approximately half as many osteoclasts ($p < 0.05$) and osteoblasts ($p < 0.05$) on the surfaces of the cortical bone in $P2Y_{13}R^{-/-}$ mice compared with WT controls (Fig. 2*A*-2*D*). In the trabecular region of the tibia, $P2Y_{13}R^{-/-}$ mice had 22% fewer osteoblasts per mm trabecular surface compared with WT controls ($p < 0.05$) (Fig. 2*E*-2*G*) though no significant reduction in osteoclast numbers.

$P2Y_{13}R^{-/-}$ mice have reduced rates of bone formation *in vivo*

To determine whether deletion of the $P2Y_{13}$ receptor would lead to reduced remodelling, 16 week-old mice were given intraperitoneal injections of calcein (30 mg/kg) 14 days and 2 days prior to being euthanized to allow for assessment of the rate and extent of mineralization (Fig. 3*A*). Comparing the $P2Y_{13}R^{-/-}$ with WT mice, the mineral apposition rate and bone formation rate were both significantly reduced by nearly 50% in the tibia ($p < 0.0001$ and $p < 0.0001$) (Fig. 3*B*+*C*).

Loss of $P2Y_{13}R$ leads to reduced osteoblast function *in vitro*

To determine whether osteoblast function is altered in $P2Y_{13}R^{-/-}$ mice, primary osteoblasts were isolated and cultured *in vitro*. There were no significant differences in the proliferation rates of $P2Y_{13}R^{-/-}$ osteoblasts compared with WT mice over a 5-day period (Fig. 4*A*). However, a 50% reduction in mineralization was observed in long term differentiation cultures compared to WT ($p < 0.0001$)(Fig. 4*B*+*C*). These data confirm that $P2Y_{13}R$ is involved in normal osteoblast function.

Loss of $P2Y_{13}R$ leads to reduced osteoclast formation *in vitro*

TRAP positive osteoclasts with three or more nuclei were identified when isolated monocytes from both WT and $P2Y_{13}R^{-/-}$ mice were cultured on glass coverslips in the presence of M-CSF and RANKL for 10 days (Fig. 4*D*, black arrows). The number of multinucleated osteoclasts formed from $P2Y_{13}R^{-/-}$ mice was 50% lower when compared with WT ($p < 0.0001$) (Fig. 4*E*). To determine the effect on osteoclast function, isolated monocytes were cultured in the presence of M-CSF and RANKL for 17 days on dentine disks and the number of resorbing osteoclasts (Fig 4*F*, black arrows) and amount of resorption were quantified (Fig 4*F*, white arrows). There were 47.1% fewer resorbing osteoclasts from $P2Y_{13}R^{-/-}$ mice ($p = 0.0004$) (Fig 4*G*) which resulted in 66% less total resorption ($p < 0.0001$) (Fig. 4*H*). However, there was no significant difference in the amount of resorption per functional, resorbing osteoclast ($p = 0.5$) (Fig. 4*I*).

Down-regulation of key regulatory genes in $P2Y_{13}R^{-/-}$ mice

To delineate the effect of *P2ry13* gene deletion on downstream signalling pathways, a TaqMan custom array was used to analyse cDNA from primary osteoblasts and long bone marrow of both $P2Y_{13}R^{-/-}$ and WT mice. Results confirmed the absence of the $P2Y_{13}$ receptor mRNA in osteoblasts and bone marrow from $P2Y_{13}R^{-/-}$ mice, further confirming successful deletion of the gene. The difference in expression for each target cDNA between the WT and $P2Y_{13}R^{-/-}$ mice was analyzed using the CT relative quantification method (33). In primary osteoblasts, compared to WT the expression of *RhoA* was significantly down-regulated (0.10 fold change) and *Tnfrsf11b* (the gene for OPG) was up-regulated (2.25 fold change) in $P2Y_{13}R^{-/-}$ mice (Fig. 4*J*). In bone marrow samples *Mapk3* (0.02 fold change), *Rock1* (0.25 fold change), *RhoA* (0.12 fold change), and *Tnfsf11* (RANKL, 0.45 fold change) were all significantly down-regulated (Fig. 4*K*).

Estrogen deficiency-induced bone loss is attenuated in $P2Y_{13}R^{-/-}$ mice

Accelerated bone loss after the menopause is a primary cause of osteoporosis in women. To determine if the reduced osteoclast function seen in $P2Y_{13}R^{-/-}$ mice may attenuate estrogen deficiency-induced bone loss, OVX surgery was performed on 4 month old mice. Four weeks after surgery, there was a

160 significant difference in the response of $P2Y_{13}R^{-/-}$ mice compared to WT mice in BMD ($p < 0.05$) and
161 trabecular thickness ($p < 0.001$). A significant loss of BMD in WT mice ($p < 0.001$) was observed at 4
162 weeks compared to baseline, but not in $P2Y_{13}R^{-/-}$ mice (Fig. 5*A*). μCT analysis of the trabecular bone
163 structure of the tibial region demonstrated significant thinning of the individual trabeculae in WT
164 mice at 4 weeks compared to baseline ($p < 0.0001$) but not in $P2Y_{13}R^{-/-}$ mice (Fig. 5*B*). Interestingly,
165 12 weeks after surgery the protection from OVX-induce bone loss in $P2Y_{13}R^{-/-}$ mice was more
166 apparent ($p < 0.001$ for both parameters compared with WT). In WT mice, BMD and trabecular
167 thickness were still reduced compared with baseline (Fig. 5*A*, $p < 0.05$ and Fig. 5*B* $p < 0.0001$
168 respectively) whereas the $P2Y_{13}R^{-/-}$ mice showed an increase in both BMD ($p < 0.05$) and trabecular
169 thickness compared with baseline levels (Fig. 5*A* and *B* respectively).
170
171

Discussion

The $P2Y_{13}$ receptor is widely distributed in different tissues and cell types, including osteoclasts and osteoblasts (30, 31). Given the emerging important role of the purinergic signalling pathway in the bone microenvironment and bone remodelling, we wanted to investigate the consequence of $P2Y_{13}$ receptor deletion on the skeleton. Deletion of $P2Y_{13}$ receptor had no effect on the gross physiology of the mice, which were healthy and fertile. When examining the bone using μCT analysis, we found that the $P2Y_{13}R^{-/-}$ mice had less bone volume in the whole tibia although the overall length was unchanged. A more detailed analysis using high resolution μCT scan was performed to determine which bone compartment was the source of the observed reduction in bone. Data obtained from the proximal tibia revealed that the $P2Y_{13}R^{-/-}$ mice had almost 40% less trabecular bone and trabecular number. The $P2Y_{13}R^{-/-}$ mice also had significantly higher trabecular pattern factor and structural model index, which indicates a less well-connected and more rod-like structured trabecular bone, in contrast to the well connected and flat structure typically seen in normal healthy animals (34, 35). There were no significant changes in any of the relevant indices for cortical bone.

To investigate further the observed bone phenotype, histomorphometric analysis demonstrated that the $P2Y_{13}R^{-/-}$ mice have half the number of osteoclasts and osteoblasts per unit of bone on the endocortical bone surface, whilst in the trabecular bone only a reduction in osteoblast numbers was observed. This imbalance in osteoblast to osteoclast numbers on the trabecular bone surface may explain the loss of trabecular bone in this region, whilst the equal reduction of both osteoblasts and osteoclasts on the cortical surface would lead to no net loss of bone. *In vitro* primary bone marrow cell cultures confirmed that deletion of the $P2Y_{13}$ receptor significantly reduced the capacity of bone marrow cells to form multinuclear, functional osteoclasts. This led to the significant decrease in total resorption observed, whereas the amount of resorption per osteoclast was not different from that of osteoclasts derived from WT bone marrow. Interestingly, primary osteoblast cultures demonstrated that the cells from $P2Y_{13}R^{-/-}$ mice had reduced function, leading to a 50% decrease in mineralization. These *in vitro* results are consistent with the 50% decrease in bone apposition rate and bone formation rate detected in $P2Y_{13}R^{-/-}$ mice using dynamic histomorphometry. Coupled with the reduction in the

number of osteoclasts this would result in an overall reduced bone remodelling rate, especially the bone formation rate, in 4 month old $P2Y_{13}R^{-/-}$ mice. Due to the relatively higher turnover activity in trabecular bone than in cortical bone (36), fewer functional osteoblasts and a lower bone formation rate will have affected trabecular bone to a greater extent than cortical bone.

Data obtained from the TaqMan custom array analysis provide possible explanations at the molecular level for the observed effect of $P2Y_{13}$ receptor deletion on osteoblasts and osteoclasts. The down-regulation of the expression of *RhoA* was found in both primary $P2Y_{13}R^{-/-}$ osteoblasts and bone marrow. There is evidence that the $P2Y_{13}R$ is upstream of the RhoA/ROCK I signalling controlling HDL endocytosis in human hepatocytes (37). Our data indicate that in addition to this acute activation of the RhoA pathway, the $P2Y_{13}$ receptor would also control the level of RhoA and ROCK1. Inhibition of RhoA/ROCK I signalling will reduce extracellular signal-regulated kinase (ERK) activity, diminish RUNX2 activity, and alter ALP activity in osteoblasts (38). Down regulation of ERK signalling via RhoA/ROCK I signalling in osteoclasts has previously been shown to impair survival and induce apoptosis in osteoclasts by affecting the formation of a ruffled border and the maintenance of cell polarity (39, 40). Interestingly, mRNA of *Mapk3* was decreased in $P2Y_{13}R^{-/-}$ bone marrow. Therefore, the deletion of $P2Y_{13}R$ may lead to the down regulation of RhoA/ROCK I signalling, which in turn affects the downstream ERK-MAPK signalling causing reduced function and differentiation of bone cells, particularly osteoblasts. The other interesting finding with the TaqMan analysis was the up-regulation of *Tnfrsf11b* (osteoprotegerin, OPG) in the $P2Y_{13}R^{-/-}$ osteoblasts and the down-regulation of *Tnfsf11* (RANKL) in $P2Y_{13}R^{-/-}$ mice bone marrow. These gene expression alterations would indicate an overall reduced ratio of RANKL/OPG and hence negative regulation of osteoclastogenesis, which may explain the phenomenon of reduced osteoclast formation observed in $P2Y_{13}R^{-/-}$ mice both *in vivo* and *in vitro*.

Osteoporosis is a condition in which there is over-activated bone turnover and in which osteoclast resorption exceeds osteoblastic bone formation leading to an overall net bone loss and bone fragility (41, 42). Bone loss accelerates in older women due to the menopause because estrogen withdrawal

increases the rate of bone remodelling - coupled with negative bone balance this produces bone loss and trabecular thinning (43). To investigate the pharmaceutical potential of lower bone turnover activities induced by the deletion of $P2Y_{13}R$, both $P2Y_{13}R^{-/-}$ and WT mice were ovariectomized to examine the bone changes under estrogen deficiency-induced osteoporosis. Four weeks after the OVX surgery, $P2Y_{13}R^{-/-}$ mice showed no significant loss of BMD, and even showed increased BMD 12-weeks after surgery. The observation that the $P2Y_{13}R^{-/-}$ mice have an attenuated response to estrogen deficiency-induced bone loss highlights this receptor as a possible new therapeutic target for osteoporosis. This is timely given the growing concern over the possible association of atypical fractures of the femur with long-term use of bisphosphonates (44). Bisphosphonates work by inhibiting the catabolic actions of osteoclasts leading to an overall suppression of bone turnover. Long term suppression of bone turnover may lead to the accumulation of microdamage in bone because of a failure to efficiently remove cracks which will ultimately lead to fracture of the bone (45). Targeting the $P2Y_{13}R$ may provide an alternative treatment which slows down the accelerated bone loss observed in post-menopausal women whilst maintaining turnover activities at a reduced rate to ensure repair of microdamage.

In conclusion, this is the first detailed study to examine the role of $P2Y_{13}$ receptor in bone homeostasis both *in vivo* and *in vitro*. Deletion of the $P2Y_{13}$ receptor leads to less trabecular bone in mice, by affecting both osteoblasts and osteoclasts. As a consequence, a lower bone apposition rate and bone formation rate were detected in 4 month old $P2Y_{13}R^{-/-}$ female mice. The down-regulation of RhoA/ROCK I signalling and a reduced ratio of RANKL/OPG may be the possible molecular mechanisms causing these bone phenotype alterations. The lower bone remodelling activity and the apparent protection from OVX-induced bone loss in $P2Y_{13}R^{-/-}$ mice suggest a possible new target for fighting bone diseases such as osteoporosis in the future.

MATERIALS AND METHODS

Mice

The strain of $P2Y_{13}$ receptor knockout ($P2Y_{13}R^{-/-}$) mouse was generated by classical homologous recombination in ES cells and aggregation with morulae as previously described (46). Briefly, the targeting of the *P2ry13* gene was obtained by replacing a 1200 bp fragment containing the first non coding exon and the first 182 bp from the ATG starting coding sequence by a neomycin-resistance cassette. Male chimeras obtained from two different ES cells colonies were used to generate the $P2Y_{13}R^{-/-}$ mouse strain. Targeting of the gene was confirmed by Southern blotting and RT-PCR. The $P2Y_{13}$ mutation was crossed on C57BL/6J background for 10 generations. $P2Y_{13}R^{-/-}$ and wild type (WT) mice were housed in the same environmentally controlled conditions with a 12hr light/dark cycle at 22°C. They were free to access *2018 Teklad* Global 18% Protein Rodent Diet containing 1.01% Calcium (Harlan Laboratories, UK) and water *ad libitum* in sterile RB-3 cages. For bone phenotype investigations, female mice were euthanized at 16 week of age. For dynamic histomorphometry, mice were given intraperitoneal injections of calcein (30 mg/kg) 14 days and 2 days prior to being euthanized. Hind limbs were dissected free of attached soft tissue for bone phenotype investigation. The lengths of tibiae were measured from the lowest point of the distal end to the highest point of the proximal end using calibrated vernier callipers. All procedures complied with the UK Animals (Scientific Procedures) Act 1986 and were reviewed and approved by the local Research Ethics Committee of the University of Sheffield (Sheffield, UK).

μCT

Right tibiae were dissected, fixed in 70% ethanol and scanned by SkyScan 1172 desktop μCT (SkyScan) at the resolution of 4.3μm for the tibia proximal end and 17.3μm for the whole tibia. The X-ray source was operated at 50kV and 200μA with a 0.5 aluminium filter. Two-dimensional CT images were captured every 0.7^{o} through 180^{o} rotation of the bone and were then reconstructed by Skyscan NRecon software at threshold of 0.0-0.16 and 0.0-0.14 for tibia proximal end and whole tibia scan respectively. Region of interest (ROI) was selected and analyzed by Skyscan CTan software. For

the proximal tibia scan, trabecular morphometry was characterized by measuring structural parameters from a 1.0mm thick trabecular abundant region which is 0.2mm below the growth plate. The parameters included the Bone Mineral density (BMD), bone volume fraction (BV/TV), trabecular thickness (Tb.Th), and trabecular number (Tb.N). Cortical bone parameters, including cortical bone volume (Ct.BV), endosteal diameter (Es. Dm), and periosteal diameter (Ps. Dm), were quantified from a 1.0mm thick predominantly cortical region 1.0mm below the growth plate.

Bone histomorphometry

The left tibiae were fixed in 10% buffered formalin, decalcified in 14.3% EDTA for 28 days, and then embedded in paraffin wax. Sections were cut (at 3µm) using a Leica Microsystems Microtome and TRAP stained as described previously (47, 48). Briefly, sections were incubated in prewarmed Acetate-tartrate buffer (0.1M Sodium tartrate (Sigma) in 0.2M Acetate buffer (Sigma), pH5.2) at 37°C for 5 mins, followed by 30 mins incubation at 37°C in 20mg/mL Naphthol AS-BI phosphate (Sigma) /Dimethylformamide (Fisher) in Acetate-tartrate buffer. The sections were then incubated in Acetate-tartrate buffer hexazotised pararosaniline solution, rinsed in water and counterstained in Gill's haematoxylin. The number of osteoblasts (N.Ob/B.Pm) and the number of osteoclasts were determined on a 3mm length of endocortical surface and a 0.75 mm^2 trabecular bone area, starting 0.25mm from the growth plate and viewed on a DMRB microscope (Leica Microsystems)(47). For dynamic histomorphometry, right tibiae were dissected and fixed in 70% ethanol, followed by embedded into LR White resin (Taab Laboratory Equipment Ltd). Sections were cut at 10µm using a Leica Microsystems Microtome. Mineral apposition rate (MAR) and the bone formation rate (BFR/BS) were obtained using a DMRB microscope as described previously (47). All histomorphometric parameters were based on the report of the ASBMR Histomorphometry nomenclature (49) and were obtained using the Osteomeasure bone histomorphometry software (Osteometrics)

Primary osteoblast isolation

Neonatal mouse calvariae (less than 72 hours old, 5-7 pups per culture) were dissected and the attached soft tissue was removed by digestion in 1mg/ml Collagenase 1A (Sigma) for 15 mins. Calvariae were then subjected to serial digestion in 1mg/mL Collagenase 1A for 30 mins; 0.25% Trypsin/EDTA (Gibco) for 30 mins; and 1mg/mL Collagenase 1A for 30 mins, at 37°C. All cells were harvested from the digestion suspensions and seeded into a T75 flask and cultured until confluent in DMEM© GLUTAMAX™ medium with sodium pyruvate (Gibco), 100 Units/mL Penicillin and 100 µg/mL Streptomycin (Gibco) and 10% foetal calf serum (FCS) (Gibco).

Proliferation Assay

First passage primary osteoblast cells isolated from $P2Y_{13}R^{-/-}$ and WT neonatal calvaria were seeded at a density of 5 $x10^3$ cells per well of a 96-well plate and cultured in DMEM© GLUTAMAX™ medium with sodium pyruvate, 100 Units/mL Penicillin and 100 µg/mL Streptomycin and 10% FCS for 5 days. On day 5, samples were examined by 3-(4,5-dimethylthiazol-2-yl) -5- (3-carboxymethoxyphenyl) -2- (4-sulfophenyl)-2H-tetrazolium, inner salt (MTS) assay (Promega) according to the manufacturer's instructions. The absorbance was read at 490nm on a SpectraMax $M5^e$ Microplate Reader (Molecular Devices).

Mineralization assay

First passage primary osteoblast cells were initially seeded at 1.5 x 10^4 cell/well in 12-well plate and cultured in growth medium for six days and changed into differentiation medium: DMEM© GLUTAMAX™ with sodium pyruvate, 100 Units/mL Penicillin and 100 µg/mL Streptomycin, 10% Fetal calf serum, 10nM Dexamethasone (Sigma), 50µg/mL L-Ascorbate Acid (Sigma), and 2mM β-glycerophosphate (Sigma)(50, 51). Cells were cultured in differentiation medium for three weeks and medium was changed every two to three days. Cells were then rinsed by PBS and fixed in 100% Ethanol for minimum 1 hr or maximum overnight at 4°C. Nodules formed by osteoblast were stained by Alizarin Red S (52). Briefly, cells after fixation were rinsed twice by PBS and incubated in 40mM alizarin red S pH 4.2 (Sigma) for 1hr at room temperature. Plates were washed with 95% ethanol on the shaker until solution became clear and air dried. The plates were then scanned using an Epson

Perfection 4990 Photo flatbed scanner (Epson Ltd, Herts, UK) and the percentage mineralisation area to the total area (Area Friction) was determined using Image J software (http://rsbweb.nih.gov/ij/). To normalize the results, the plates were re-hydrated using PBS and counterstained for 10-15 Sec with 0.1% Toluidine blue. The plates were scanned and the total areas covered by cells were quantified using Image J software. The mineralization results were then normalized to the Toluidine blue staining results of their relevant wells.

Primary Osteoclast isolation

Osteoclasts were derived from the mononuclear hematopoietic cell population from the long bone marrow of 10 weeks old female mice. Mononuclear cells were isolated using a modified protocol to that previously described (53). In brief, the bone marrow of limbs was flushed out by PBS using a syringe with 25-gauge needle. Cells were harvested by centrifugation and resuspended in the selection medium (Alpha-Minimal essential medium (α MEM) + GLUTAMAX™ (Gibco), 100 Units/mL Penicillin/100 µg/mL Streptomycin, 10% FCS, and 50ng/ml murine macrophage colony stimulating factor (M-CSF). The cells were then transferred into a T75 flask and incubated for 24 hours at 37°C, 5% CO_2 to allow the attachment of stromal cells. Non-adherent cells were collected by centrifugation and resuspended in growth medium (α MEM+GLUTAMAX™ containing 100 Units/mL Penicillin and 100 µg/mL Streptomycin, 10% FCS, 25ng/ml M-CSF, and 3ng/ml murine receptor activator of NF-κB ligand (RANKL) (R&D System)). The cells were then seeded onto glass coverslips ((Richardson's of Leicester) or dentine disks (www.dentinedisks.com) in 96-well plates at density of $1x10^6$ cells per well and cultured at 37°C, 7% CO_2 with the medium being replaced every 2-3 days. Cells on coverslips were cultured for 10 days and fixed in ice cold 10% buffered formalin, whereas cells on dentine disks were cultured for 17 days to allow time for resorption. Both coverslips and dentine disks were TRAP stained and counterstained by Gill's haematoxylin as described above (47). On coverslips, TRAP positive cells with more than 3 nuclei were quantified as osteoclasts. On dentine disks, the number of resorbing osteoclasts (defined as a TRAP positive cell in or in close proximity to resorption pits) and the amount of resorption per dentine disk were quantified by point-counting as previously described (54, 55).

TaqMan® Custom Array

Total RNA was isolated from both primary osteoblasts and long bone marrow with TRI Reagent (Sigma) according to manufacturer's instruction. Extracted RNA was quantified using a NanoDrop® ND-1000 Spectophotometer (The Thermo Scientific) and RNA quality was checked using an Agilent 2100 Bioanalyzer (Agilent Technologies). The cDNA was then synthesized using Promega ImProm-II™ reverse trancriptase (Promega) with Oligo(dT) 15 primer (Promega) according to manufacturer's instruction. An Applied Biosystems TaqMan custom array was used to validate the differential expression of candidate genes. The quantitative RT-PCR amplification of the TaqMan arrays were performed on an Applied Biosystems 7900HT Real-Time PCR system (Applied Biosystems) with thermal cycling conditions: 2 mins at 50°C, 10 mins at 94.5°C, followed by 40 cycles of denaturation at 97°C for 30 sec and extension at 59.7°C for 1 min (56). Data was collected and analysed using the Applied Biosystems SDS 2.2.1 software (Applied Biosystems). In order to systematically compare all target genes and limit interpolated errors, the same threshold values of 0.2 was used for each gene. The data were then analyzed using the CT relative quantification method (33). Quantification of the target cDNAs in all samples was normalized to the endogenous control gene: β-actin (*Actb*) ($\Delta CT = CT_{target} - CT_{Actb}$). The difference in expression for each target cDNA between the WT and $P2Y_{13}R^{-/-}$ mice was expressed as ΔΔCT ($\Delta\Delta CT = \Delta CT_{WT} - \Delta CT_{P2Y13R-/-}$). Fold changes in target genes were calculated by taking 2 to the power of the ΔΔCT ($2^{\Delta\Delta CT}$). Any genes with more than two folds expression changes were recognized as significant variance (57). A heatmap showing gene expression pattern variance was built from normalized ΔΔCT values, using the 'GenePattern' web software (http://www.broadinstitute.org). Each colour patch in the heatmap represents the relative gene expression level, with a continuum of expression levels from dark blue (lowest) to bright red (highest).

OVX surgery

OVX or sham-OVX (SHAM) surgery was performed on 16 weeks old, virgin, female WT and $P2Y_{13}R^{-/-}$ mice (n = 7-9/group). OVX and SHAM surgery were performed as previously described

(58). Briefly, mice were anesthetized with 1.5-4% isoflurane in oxygen for surgery. The back of each mouse was shaved and surrounding area was cleaned with 70% ethanol. Dorsal incision was made through the skin in the region between the dorsal hump and the base of the tail. The ovaries, surrounding ovarian fat pad, and part of uterine horns under the abdomen wall were removed. For sham surgery, the ovaries and proximal parts of the uterine horns were exteriorised briefly then returned to the abdominal cavity before wound closure. Mice were euthanized for bone phenotype examination 4 weeks and 12 weeks after surgery to investigate bone phenotype changes.

Statistic analysis

All data are expressed as mean ± SEM. Statistical significance was tested for using either univariate analysis of variance or an unpaired Student's t-test using PASW Statistics (IBM, NY) and Prism 5 software (GraphPad, La Jolla).

Acknowledgements

The authors would like to thank the staff of the Bone Analysis Laboratory, The University of Sheffield for tissues processing and TRAP staining. This study was supported by the European Commission under the 7th Framework Programme (proposal #202231) performed as a collaborative project among the members of the ATPBone Consortium (Copenhagen University, University College London, University of Maastricht, University of Ferrara, University of Liverpool, University of Sheffield, and Université Libre de Bruxelles), and is a sub study under the main study "Fighting osteoporosis by blocking nucleotides: purinergic signalling in bone formation and homeostasis".

References:

1. Burnstock G 2007 Purine and pyrimidine receptors. Cell Mol Life Sci 64:1471-1483
2. Orriss IR, Knight GE, Ranasinghe S, Burnstock G, Arnett TR 2006 Osteoblast responses to nucleotides increase during differentiation. Bone 39:300-309
3. Dixon CJ, Bowler WB, Walsh CA, Gallagher JA 1997 Effects of extracellular nucleotides on single cells and populations of human osteoblasts: contribution of cell heterogeneity to relative potencies. Br J Pharmacol 120:777-780
4. Nakamura E, Uezono Y, Narusawa K, Shibuya I, Oishi Y, Tanaka M, Yanagihara N, Nakamura T, Izumi F 2000 ATP activates DNA synthesis by acting on P2X receptors in human osteoblast-like MG-63 cells. Am J Physiol Cell Physiol 279:C510-519
5. Buckley KA, Hipskind RA, Gartland A, Bowler WB, Gallagher JA 2002 Adenosine triphosphate stimulates human osteoclast activity via upregulation of osteoblast-expressed receptor activator of nuclear factor-kappa B ligand. Bone 31:582-590
6. Buckley KA, Wagstaff SC, McKay G, Gaw A, Hipskind RA, Bilbe G, Gallagher JA, Bowler WB 2001 Parathyroid hormone potentiates nucleotide-induced [Ca2+]i release in rat osteoblasts independently of Gq activation or cyclic monophosphate accumulation. A mechanism for localizing systemic responses in bone. J Biol Chem 276:9565-9571
7. Korcok J, Raimundo LN, Du X, Sims SM, Dixon SJ 2005 P2Y6 nucleotide receptors activate NF-kappaB and increase survival of osteoclasts. J Biol Chem 280:16909-16915
8. Morrison MS, Turin L, King BF, Burnstock G, Arnett TR 1998 ATP is a potent stimulator of the activation and formation of rodent osteoclasts. J Physiol 511 (Pt 2):495-500
9. Agrawal A, Buckley KA, Bowers K, Furber M, Gallagher JA, Gartland A 2010 The effects of P2X7 receptor antagonists on the formation and function of human osteoclasts in vitro. Purinergic Signal 6:307-315
10. Gartland A, Buckley KA, Bowler WB, Gallagher JA 2003 Blockade of the pore-forming P2X7 receptor inhibits formation of multinucleated human osteoclasts in vitro. Calcif Tissue Int 73:361-369

11. Hoebertz A, Meghji S, Burnstock G, Arnett TR 2001 Extracellular ADP is a powerful osteolytic agent: evidence for signaling through the P2Y(1) receptor on bone cells. Faseb J 15:1139-1148

12. Orriss IR, Utting JC, Brandao-Burch A, Colston K, Grubb BR, Burnstock G, Arnett TR 2007 Extracellular nucleotides block bone mineralization in vitro: evidence for dual inhibitory mechanisms involving both P2Y2 receptors and pyrophosphate. Endocrinology 148:4208-4216

13. Gartland A, Buckley KA, Hipskind RA, Perry MJ, Tobias JH, Buell G, Chessell I, Bowler WB, Gallagher JA 2003 Multinucleated osteoclast formation in vivo and in vitro by P2X7 receptor-deficient mice. Crit Rev Eukaryot Gene Expr 13:243-253

14. Ke HZ, Qi H, Weidema AF, Zhang Q, Panupinthu N, Crawford DT, Grasser WA, Paralkar VM, Li M, Audoly LP, Gabel CA, Jee WS, Dixon SJ, Sims SM, Thompson DD 2003 Deletion of the P2X7 nucleotide receptor reveals its regulatory roles in bone formation and resorption. MolEndocrinol 17:1356-1367

15. Orriss I, Syberg S, Wang N, Robaye B, Gartland A, Jorgensen N, Arnett T, Boeynaems J-M 2011 Bone phenotypes displayed by P2 receptor knockout mice. Frontiers in Bioscience

16. Wittenberger T, Schaller HC, Hellebrand S 2001 An expressed sequence tag (EST) data mining strategy succeeding in the discovery of new G-protein coupled receptors. J Mol Biol 307:799-813

17. Communi D, Gonzalez NS, Detheux M, Brezillon S, Lannoy V, Parmentier M, Boeynaems JM 2001 Identification of a novel human ADP receptor coupled to G(i). J Biol Chem 276:41479-41485

18. Zhang FL, Luo L, Gustafson E, Palmer K, Qiao X, Fan X, Yang S, Laz TM, Bayne M, Monsma F, Jr. 2002 P2Y(13): identification and characterization of a novel Galphai-coupled ADP receptor from human and mouse. J Pharmacol Exp Ther 301:705-713

19. Fumagalli M, Trincavelli L, Lecca D, Martini C, Ciana P, Abbracchio MP 2004 Cloning, pharmacological characterisation and distribution of the rat G-protein-coupled P2Y(13) receptor. Biochem Pharmacol 68:113-124

20. Queiroz G, Talaia C, Goncalves J 2003 ATP modulates noradrenaline release by activation of inhibitory P2Y receptors and facilitatory P2X receptors in the rat vas deferens. J Pharmacol Exp Ther 307:809-815

21. Grimm I, Messemer N, Stanke M, Gachet C, Zimmermann H 2009 Coordinate pathways for nucleotide and EGF signaling in cultured adult neural progenitor cells. J Cell Sci 122:2524-2533

22. Csolle C, Heinrich A, Kittel A, Sperlagh B 2008 P2Y receptor mediated inhibitory modulation of noradrenaline release in response to electrical field stimulation and ischemic conditions in superfused rat hippocampus slices. J Neurochem 106:347-360

23. Heinrich A, Kittel A, Csolle C, Sylvester Vizi E, Sperlagh B 2008 Modulation of neurotransmitter release by P2X and P2Y receptors in the rat spinal cord. Neuropharmacology 54:375-386

24. Wang L, Olivecrona G, Gotberg M, Olsson ML, Winzell MS, Erlinge D 2005 ADP acting on P2Y13 receptors is a negative feedback pathway for ATP release from human red blood cells. Circ Res 96:189-196

25. Carrasquero LM, Delicado EG, Bustillo D, Gutierrez-Martin Y, Artalejo AR, Miras-Portugal MT 2009 P2X7 and P2Y13 purinergic receptors mediate intracellular calcium responses to BzATP in rat cerebellar astrocytes. J Neurochem 110:879-889

26. Marteau F, Le Poul E, Communi D, Communi D, Labouret C, Savi P, Boeynaems JM, Gonzalez NS 2003 Pharmacological characterization of the human P2Y13 receptor. Mol Pharmacol 64:104-112

27. Jacquet S, Malaval C, Martinez LO, Sak K, Rolland C, Perez C, Nauze M, Champagne E, Terce F, Gachet C, Perret B, Collet X, Boeynaems JM, Barbaras R 2005 The nucleotide receptor P2Y13 is a key regulator of hepatic high-density lipoprotein (HDL) endocytosis. Cell Mol Life Sci 62:2508-2515

28. Blom D, Yamin TT, Champy MF, Selloum M, Bedu E, Carballo-Jane E, Gerckens L, Luell S, Meurer R, Chin J, Mudgett J, Puig O 2010 Altered lipoprotein metabolism in P2Y(13) knockout mice. Biochim Biophys Acta 1801:1349-1360

29. Fabre AC, Malaval C, Ben Addi A, Verdier C, Pons V, Serhan N, Lichtenstein L, Combes G, Huby T, Briand F, Collet X, Nijstad N, Tietge UJ, Robaye B, Perret B, Boeynaems JM, Martinez LO 2010 P2Y13 receptor is critical for reverse cholesterol transport. Hepatology 52:1477-1483

30. Alvarenga EC, Rodrigues R, Caricati-Neto A, Silva-Filho FC, Paredes-Gamero EJ, Ferreira AT 2010 Low-intensity pulsed ultrasound-dependent osteoblast proliferation occurs by via activation of the P2Y receptor: role of the P2Y1 receptor. Bone 46:355-362

31. Orriss IR, Burnstock G, Arnett TR 2010 Purinergic signalling and bone remodelling. Curr Opin Pharmacol 10:322-330

32. Iwaniec UT, Yuan D, Power RA, Wronski TJ 2006 Strain-dependent variations in the response of cancellous bone to ovariectomy in mice. J Bone Miner Res 21:1068-1074

33. Livak KJ, Schmittgen TD 2001 Analysis of relative gene expression data using real-time quantitative PCR and the 2(-Delta Delta C(T)) Method. Methods 25:402-408

34. Hahn M, Vogel M, Pompesius-Kempa M, Delling G 1992 Trabecular bone pattern factor--a new parameter for simple quantification of bone microarchitecture. Bone 13:327-330

35. Hildebrand T, Ruegsegger P 1997 Quantification of Bone Microarchitecture with the Structure Model Index. Comput Methods Biomech Biomed Engin 1:15-23

36. Goodyear SR, Gibson IR, Skakle JM, Wells RP, Aspden RM 2009 A comparison of cortical and trabecular bone from C57 Black 6 mice using Raman spectroscopy. Bone 44:899-907

37. Malaval C, Laffargue M, Barbaras R, Rolland C, Peres C, Champagne E, Perret B, Terce F, Collet X, Martinez LO 2009 RhoA/ROCK I signalling downstream of the P2Y13 ADP-receptor controls HDL endocytosis in human hepatocytes. Cell Signal 21:120-127

38. Khatiwala CB, Kim PD, Peyton SR, Putnam AJ 2009 ECM compliance regulates osteogenesis by influencing MAPK signaling downstream of RhoA and ROCK. J Bone Miner Res 24:886-898

39. Idris A, Mrak E, Greig I, Guidobono F, Ralston SH, van 't Hof R 2008 ABD56 causes osteoclast apoptosis by inhibiting the NFkappaB and ERK pathways. Biochem Biophys Res Commun 371:94-98

525 40. Nakamura H, Hirata A, Tsuji T, Yamamoto T 2003 Role of osteoclast extracellular signal-
526 regulated kinase (ERK) in cell survival and maintenance of cell polarity. J Bone Miner Res
527 18:1198-1205
528 41. Garnero P, Sornay-Rendu E, Chapuy MC, Delmas PD 1996 Increased bone turnover in late
529 postmenopausal women is a major determinant of osteoporosis. J Bone Miner Res 11:337-349
530 42. Delmas PD, Eastell R, Garnero P, Seibel MJ, Stepan J 2000 The use of biochemical markers
531 of bone turnover in osteoporosis. Committee of Scientific Advisors of the International
532 Osteoporosis Foundation. Osteoporos Int 11 Suppl 6:S2-17
533 43. Seeman E 2003 Invited Review: Pathogenesis of osteoporosis. J Appl Physiol 95:2142-2151
534 44. Shane E, Burr D, Ebeling PR, Abrahamsen B, Adler RA, Brown TD, Cheung AM, Cosman F,
535 Curtis JR, Dell R, Dempster D, Einhorn TA, Genant HK, Geusens P, Klaushofer K, Koval K,
536 Lane JM, McKiernan F, McKinney R, Ng A, Nieves J, O'Keefe R, Papapoulos S, Sen HT,
537 van der Meulen MC, Weinstein RS, Whyte M 2010 Atypical subtrochanteric and diaphyseal
538 femoral fractures: report of a task force of the American Society for Bone and Mineral
539 Research. J Bone Miner Res 25:2267-2294
540 45. Odvina CV, Levy S, Rao S, Zerwekh JE, Rao DS Unusual mid-shaft fractures during long-
541 term bisphosphonate therapy. Clin Endocrinol (Oxf) 72:161-168
542 46. Fabre AC, Malaval C, Ben Addi A, Verdier N, Pons V, Serhan N, Lichtenstein L, Guillaume
543 C, Nijstad N, Tietge U, Briand F, Collet X, Robaye B, Perret B, Boeynaems JM, Martinez LO
544 2010 P2Y13 Receptor is critical for reverse cholesterol transport. Hepatology 52: 1477-1483
545 47. Heath DJ, Chantry AD, Buckle CH, Coulton L, Shaughnessy JD, Jr., Evans HR, Snowden JA,
546 Stover DR, Vanderkerken K, Croucher PI 2009 Inhibiting Dickkopf-1 (Dkk1) removes
547 suppression of bone formation and prevents the development of osteolytic bone disease in
548 multiple myeloma. J Bone Miner Res 24:425-436
549 48. van't Hof RJ, Tuinenburg-Bol Raap AC, Nijweide PJ 1995 Induction of osteoclast
550 characteristics in cultured avian blood monocytes; modulation by osteoblasts and 1,25-(OH)2
551 vitamin D3. Int J Exp Pathol 76:205-214

552 49. Parfitt AM, Drezner MK, Glorieux FH, Kanis JA, Malluche H, Meunier PJ, Ott SM, Recker
553 RR 1987 Bone histomorphometry: standardization of nomenclature, symbols, and units.
554 Report of the ASBMR Histomorphometry Nomenclature Committee. J Bone Miner Res
555 2:595-610
556 50. Orriss IR, Key ML, Colston KW, Arnett TR 2009 Inhibition of osteoblast function in vitro by
557 aminobisphosphonates. J Cell Biochem 106:109-118
558 51. Orriss IR, Knight GE, Utting JC, Taylor SE, Burnstock G, Arnett TR 2009 Hypoxia
559 stimulates vesicular ATP release from rat osteoblasts. J Cell Physiol 220:155-162
560 52. Paul H, Reginato AJ, Schumacher HR 1983 Alizarin red S staining as a screening test to
561 detect calcium compounds in synovial fluid. Arthritis Rheum 26:191-200
562 53. Arnett TR, Gibbons DC, Utting JC, Orriss IR, Hoebertz A, Rosendaal M, Meghji S 2003
563 Hypoxia is a major stimulator of osteoclast formation and bone resorption. J Cell Physiol
564 196:2-8
565 54. Walsh CA, Beresford JN, Birch MA, Boothroyd B, Gallagher JA 1991 Application of
566 reflected light microscopy to identify and quantitate resorption by isolated osteoclasts. J Bone
567 Miner Res 6:661-671
568 55. Carron JA, Walsh CA, Fraser WD, Gallagher JA 1995 Thrombospondin promotes resorption
569 by osteoclasts in vitro. Biochem Biophys Res Commun 213:1017-1025
570 56. Marionneau C, Couette B, Liu J, Li H, Mangoni ME, Nargeot J, Lei M, Escande D,
571 Demolombe S 2005 Specific pattern of ionic channel gene expression associated with
572 pacemaker activity in the mouse heart. J Physiol 562:223-234
573 57. Chu X, Strauss JR, Mariano MA, Li J, Newton DJ, Cai X, Wang RW, Yabut J, Hartley DP,
574 Evans DC, Evers R 2006 Characterization of Mice Lacking the Multidrug Resistance Protein
575 Mrp2 (Abcc2). The Journal of Pharmacology and Experimental Therapeutics 317:579-589
576 58. Govoni KE, Wergedal JE, Chadwick RB, Srivastava AK, Mohan S 2008 Prepubertal OVX
577 increases IGF-I expression and bone accretion in C57BL/6J mice. Am J Physiol Endocrinol
578 Metab 295:E1172-1180
579

580 **TABLE. 1.** Quantitative results of tibia bone parameters by μCT analysis.

	WT *n=8*	*$P2Y_{13}R^{-/-}$* *n=7*	*Means difference*	*P value summary*
BMD (g/cm^3)	1.15 ± 0.007	1.15 ± 0.010	↑0.2%	
BV/TV	9.17 ± 0.340	5.73 ± 0.634	↓37.5%	C
BV (mm^3)	0.15 ± 0.006	0.09 ± 0.010	↓36.1%	C
BS/BV (1/mm)	87.26 ± 1.428	91.14 ± 3.226	↑4.5%	
Tb.Th (mm)	0.048 ± 0.0006	0.049 ± 0.0018	↑0.8%	
Tb.N (1/mm)	1.89 ± 0.054	1.18 ± 0.132	↓37.8%	C
Tb.Pf (1/mm)	26.18 ± 0.992	31.81 ± 1.607	↑21.5%	B
Tb.Sp (mm)	0.23 ± 0.003	0.33 ± 0.024	↑43.2%	C
DA	2.49 ± 0.078	1.94 ± 0.051	↓ 22.0%	C
SMI	2.13 ± 0.031	2.41 ± 0.074	↑13.0%	B
Ct.BV (mm^3)	0.83 ± 0.016	0.88 ± 0.029	↑7.1%	
Es. Dm (mm)	1.29 ± 0.028	1.32 ± 0.018	↑2.2%	
Ps.Dm (mm)	1.69 ± 0.029	1.71 ± 0.021	↑1.6%	

581
582 Values are mean ± SEM
583 [b] $p < 0.01$ (Student's unpaired *t*-test)
584 [c] $p < 0.001$ (Student's unpaired *t*-test)
585
586
587

List of Figure Legends

FIG.1. $P2Y_{13}R^{-/-}$ mice have reduced bone volume.

(A) 3D models of whole tibiae from $P2Y_{13}R^{-/-}$ and WT animals were constructed from μCT images. No obvious morphological differences were found between the $P2Y_{13}R^{-/-}$ and WT tibia, scale bar = 2.0mm. **(B)** 3D models of the trabecular region of the tibiae were constructed from μCT images, scale bar = 0.5 mm. **(C)** μCT data analysis showed $P2Y_{13}R^{-/-}$ mice had 5.5% less total tibial bone volume, **(D)** 37.5% less trabecular bone volume, and **(E)** 37.8% fewer trabeculae than WT mice. All values are mean ± SEM, $P2Y_{13}R^{-/-}$ n = 7, WT n = 8, ^{c} $p < 0.001$ (Student's unpaired *t*-test).

FIG.2. $P2Y_{13}R^{-/-}$ mice have reduced numbers of osteoclasts and osteoblasts on the endocortical bone surface.

Left tibiae were obtained from 16 week old female mice, sections prepared and TRAP stained as previously described (47). **(A)** Black arrows indicate TRAP positive osteoclasts on endocortical surface of both WT and $P2Y_{13}R^{-/-}$ mice, scale bar = 50 μm. **(B)** $P2Y_{13}R^{-/-}$ mice had 48.1% reduction in osteoclast numbers per mm endocortical surface (N.Oc/B.Pm = 2.8 ± 0.45 versus 5.4 ± 0.75, p = 0.0136)**.** **(C)** Cobblestone-like osteoblasts with large nuclei were also identified on endocortical surface and marked with black arrow heads, scale bar = 50 μm. **(D)** $P2Y_{13}R^{-/-}$ mice had 42.6% decrease in osteoblast number per mm endocortical surface (N.Ob/B.Pm = 9.1 ± 1.47 versus 15.9 ± 2.00, p = 0.0227) compared with WT controls. **(E)** TRAP positive osteoclasts (black arrowheads) and osteoblasts (black arrows) were identified on the trabecular surface of both WT and $P2Y_{13}R^{-/-}$ mice, scale bar = 50 μm. **(F)** $P2Y_{13}R^{-/-}$ mice had 22.9% decreased osteoblast numbers per mm trabecular bone surface (N.Ob/B.Pm = 13.5 ± 0.98 versus 17.4 ± 1.09, p = 0.0213). **(G)** There was no significant difference in osteoclast numbers on the trabecular bone surface (N.Oc/B.Pm =10.0 ± 1.39 versus 10.5 ± 0.47, p = 0.7587). All values are mean ± SEM, n = 6, ^{a} $p < 0.05$, ^{b} $p < 0.01$ (Student's unpaired *t*-test).

FIG.3. $P2Y_{13}R^{-/-}$ mice have reduced rates of bone formation *in vivo*

For dynamic histomorphometry, 16 weeks-old mice were given intraperitoneal injections of calcein (30 mg/kg) 14 days and 2 days prior to being euthanized. Right tibiae were obtained and LR White resin sections prepared. **(A)** First calcein label (white arrowheads) and second calcein label (white arrows) were both detected on the endocortical bone surface from both WT and $P2Y_{13}R^{-/-}$ mice. The average width between the labels (W) were measured and used to calculate mineral apposition rate. M: bone marrow; Ct: cortical bone; scale bar = 50 μm. **(B)** Mineral apposition rate was 49.7% less on the endocortical bone surface of $P2Y_{13}R^{-/-}$ mice tibia compared to WT (MAR = 1.53 ± 0.060 versus 3.03 ± 0.194, $p < 0.0001$). **(C)** Bone formation rate of $P2Y_{13}R^{-/-}$ mice was significantly decreased by 48.9% compared to WT (BFR = 1.09 ± 0.047 versus 2.13 ± 0.167, $p < 0.0001$). All values are mean ± SEM, n = 6, ^{c} $p < 0.001$ (Student's unpaired *t*-test).

FIG.4. $P2Y_{13}R^{-/-}$ mice have reduced osteoblast function and osteoclast formation *in vitro* due to altered expressions of key bone remodelling related genes

(A) Primary osteoblast cells isolated from neonatal mice calvariae of both WT and $P2Y_{13}R^{-/-}$ mice show no significant difference in proliferation. **(B)** $P2Y_{13}R^{-/-}$ osteoblasts showed a 50.1% reduction in mineralized area compared to osteoblasts from WT mice. **(C)** Representative whole well images of primary osteoblast cells cultured in differentiation medium for three weeks and stained with alizarin red S solution to reveal mineralisation, scale bar = 5.0 mm. All values are mean ± SEM, n = 3 repeat experiments with 12 replicates per experiment, ^{c} $p < 0.001$, (Univariate analysis of variance). **(D+E)** The number of osteoclasts (defined as TRAP positive cells (pink coloured) with three or more nuclei, black arrows), derived from M-CSF and RANKL treated $P2Y_{13}R^{-/-}$ mice bone marrow and cultured on glass coverslips, was 49.5% less than that from WT, scale bar = 50 μm. **(F+G)** There were 47.1% fewer resorbing osteoclasts [identified as TRAP positive cells (black arrows) in or in close proximity to resorption pits (white arrows)] formed from $P2Y_{13}R^{-/-}$ mice, scale bar = 100 μm. **(H)** This led to 66.1% less resorption on the dentine disks compared to WT osteoclasts. **(I)** There was no significant difference in the amount of resorption per resorbing osteoclast, $p = 0.4959$. All values are mean ± SEM, n = 4, each repeat contains 6 replicates, ^{c} $p < 0.001$, (Student's unpaired *t*-test). **(J+K)** The relative gene expression pattern variance was shown in a heatmap of normalized ΔΔCT values from

643 TaqMan custom array; each colour patch in the heatmap represents the relative gene expression level,
644 with a continuum of expression levels from dark blue (lowest) to bright red (highest). Compared to
645 WT primary osteoblasts, the expression of *RhoA* in $P2Y_{13}R^{-/-}$ osteoblasts was significantly down-
646 regulated while *Tnfrsf11b* (the gene for OPG) was up-regulated. *Mapk3, Rock1*, *RhoA*, and *Tnfsf11*
647 (the gene for RANKL) were significantly down-regulation in $P2Y_{13}R^{-/-}$ bone marrow samples
648 compared to WT. No other key regulatory genes had changes in expression levels.
649
650 **FIG.5. $P2Y_{13}R^{-/-}$ mice have a reduced estrogen deficiency-induced bone loss**
651 OVX surgery was performed on 16 week-old WT and $P2Y_{13}R^{-/-}$ mice. Mice were euthanized 4 and 12
652 weeks after surgery and right tibiae were isolated and examined using μCT (Skyscan 1172). The
653 response of $P2Y_{13}R^{-/-}$ mice to OVX was different for both BMD and trabecular thickness compared
654 with WT at both time points. **(A)** WT mice had a significant reduction in BMD 4 weeks and 12 weeks
655 after surgery, no significant reduction in BMD was observed in $P2Y_{13}R^{-/-}$ mice at 4 weeks and a
656 significant increase was observed at 12 weeks. **(B)** Trabecular thickness significantly decreased in
657 WT mice both at 4 and 12 weeks after surgery, no significant reduction in thickness was observed in
658 $P2Y_{13}R^{-/-}$ mice at 4 weeks and an increase was observed at 12 weeks. All values are mean ± SEM, n =
659 7-9, * $p < 0.05$ *cf* WT, *** $p < 0.0001$ *cf* WT; ^{a} $p < 0.05$ *cf* baseline, ^{c} $p < 0.0001$ *cf* baseline; (Student's
660 unpaired *t*-test).
661

662 Figure 1

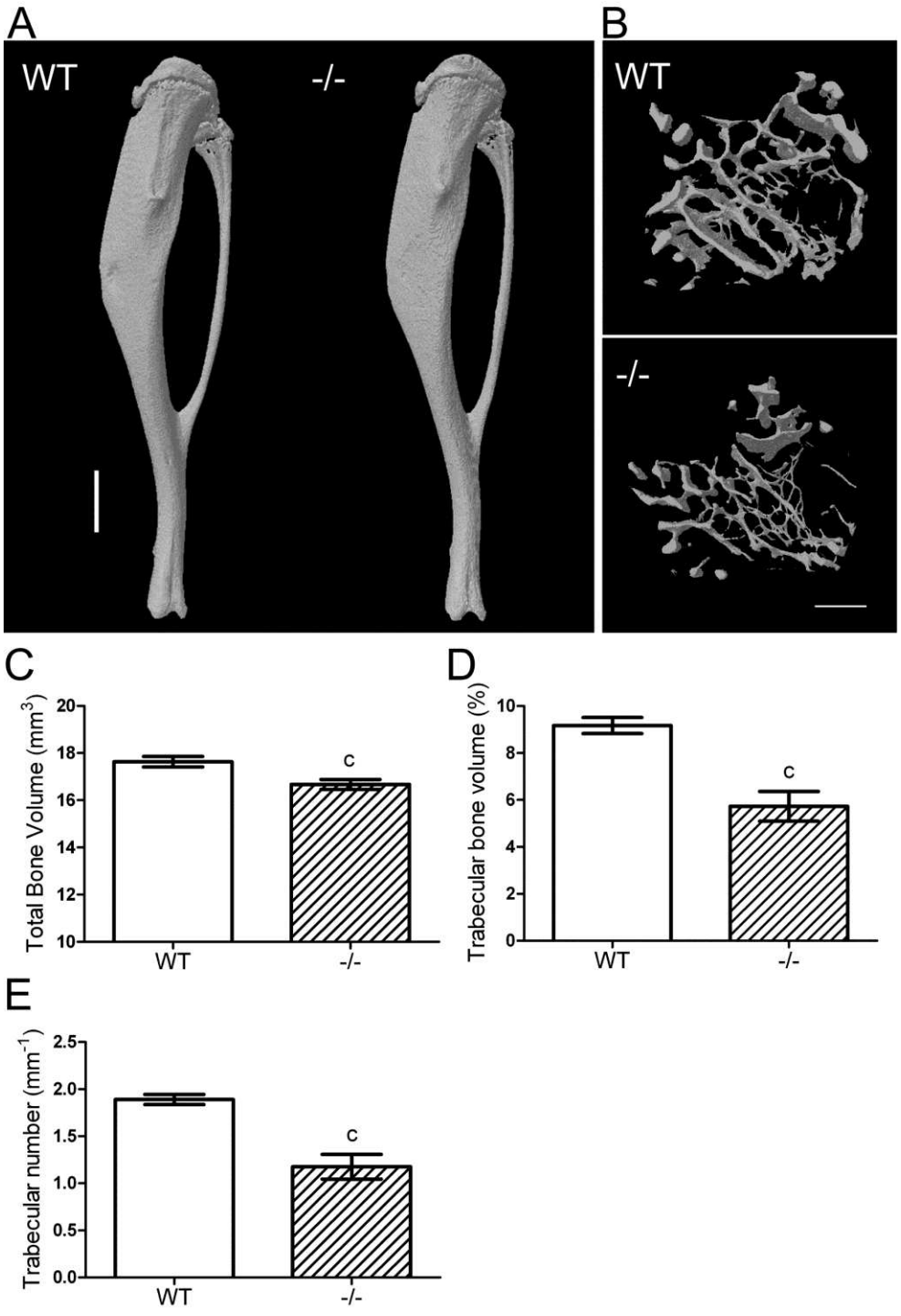

663

664

Figure 2

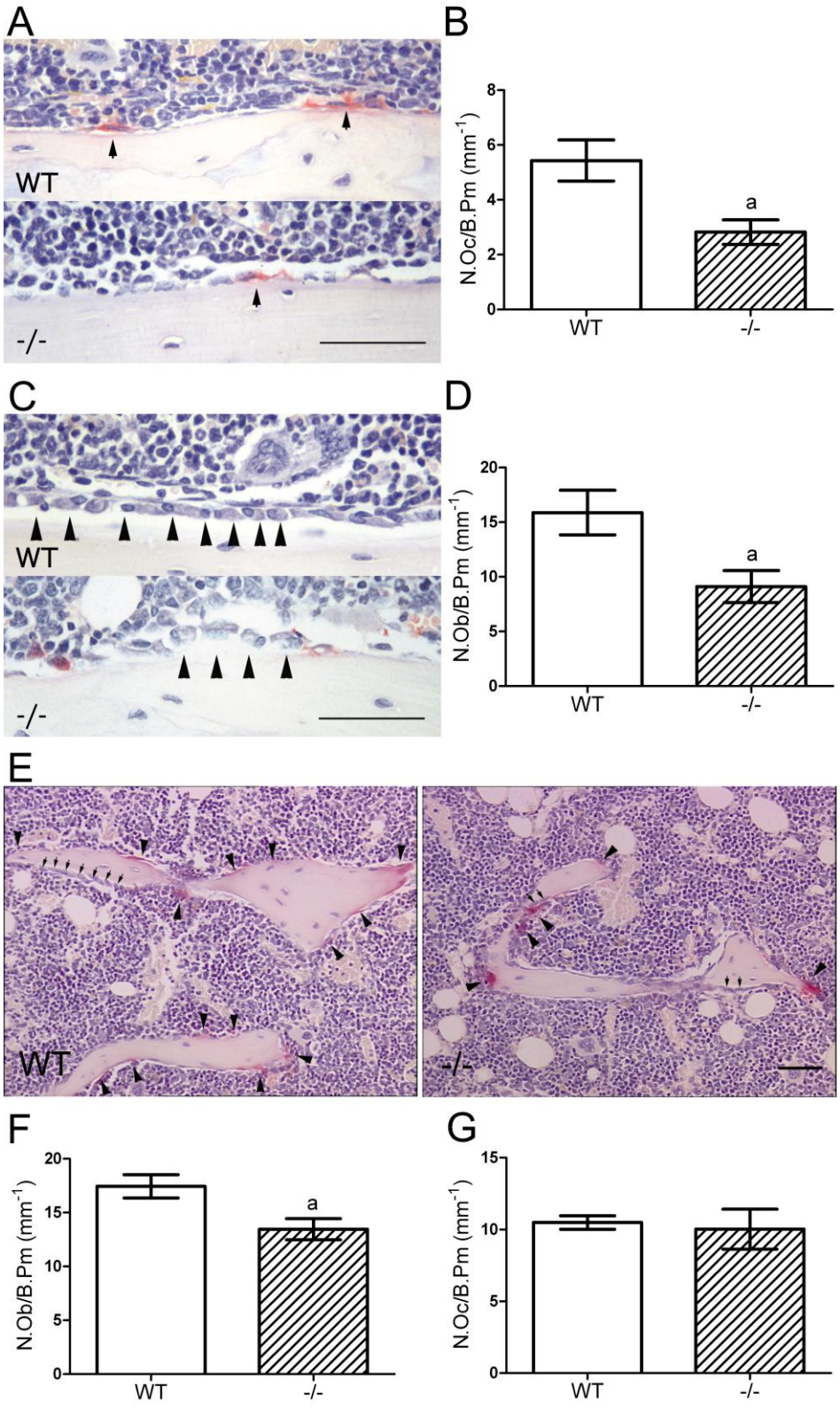
A
WT
-/-
B
N.Oc/B.Pm (mm-1)
a
WT
-/-
C
WT
-/-
D
N.Ob/B.Pm (mm-1)
a
WT
-/-
E
WT
-/-
F
N.Ob/B.Pm (mm-1)
a
WT
-/-
G
N.Oc/B.Pm (mm-1)
WT
-/-

668 Figure 3

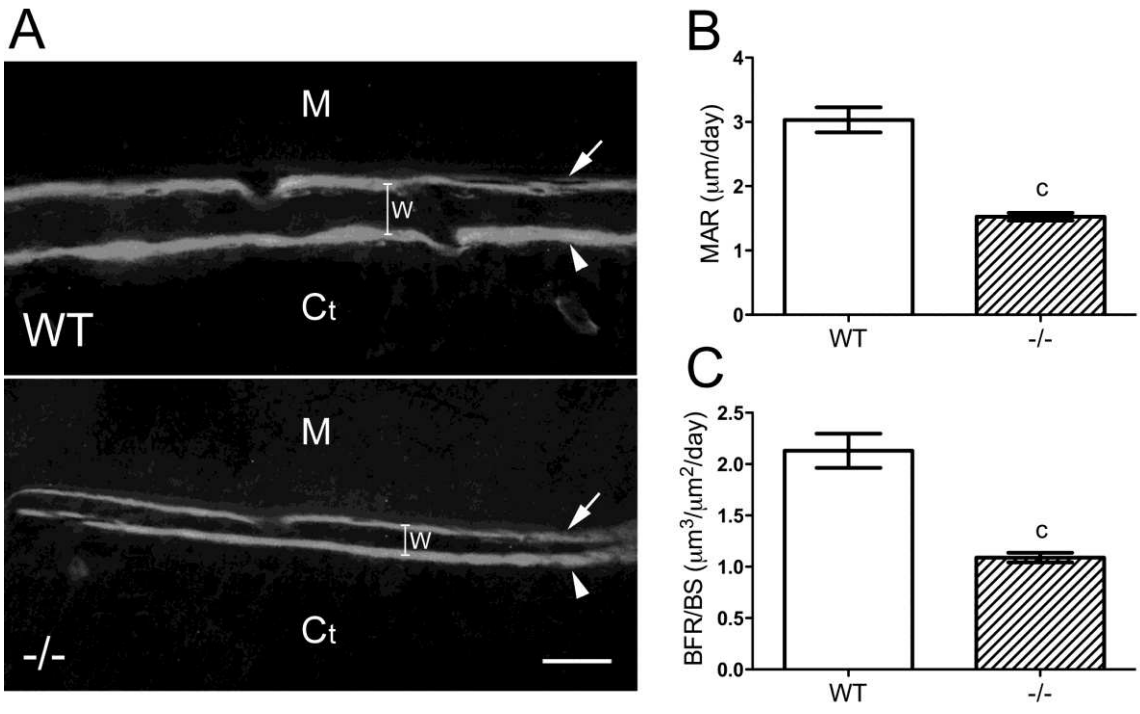

669

670

671 Figure 4

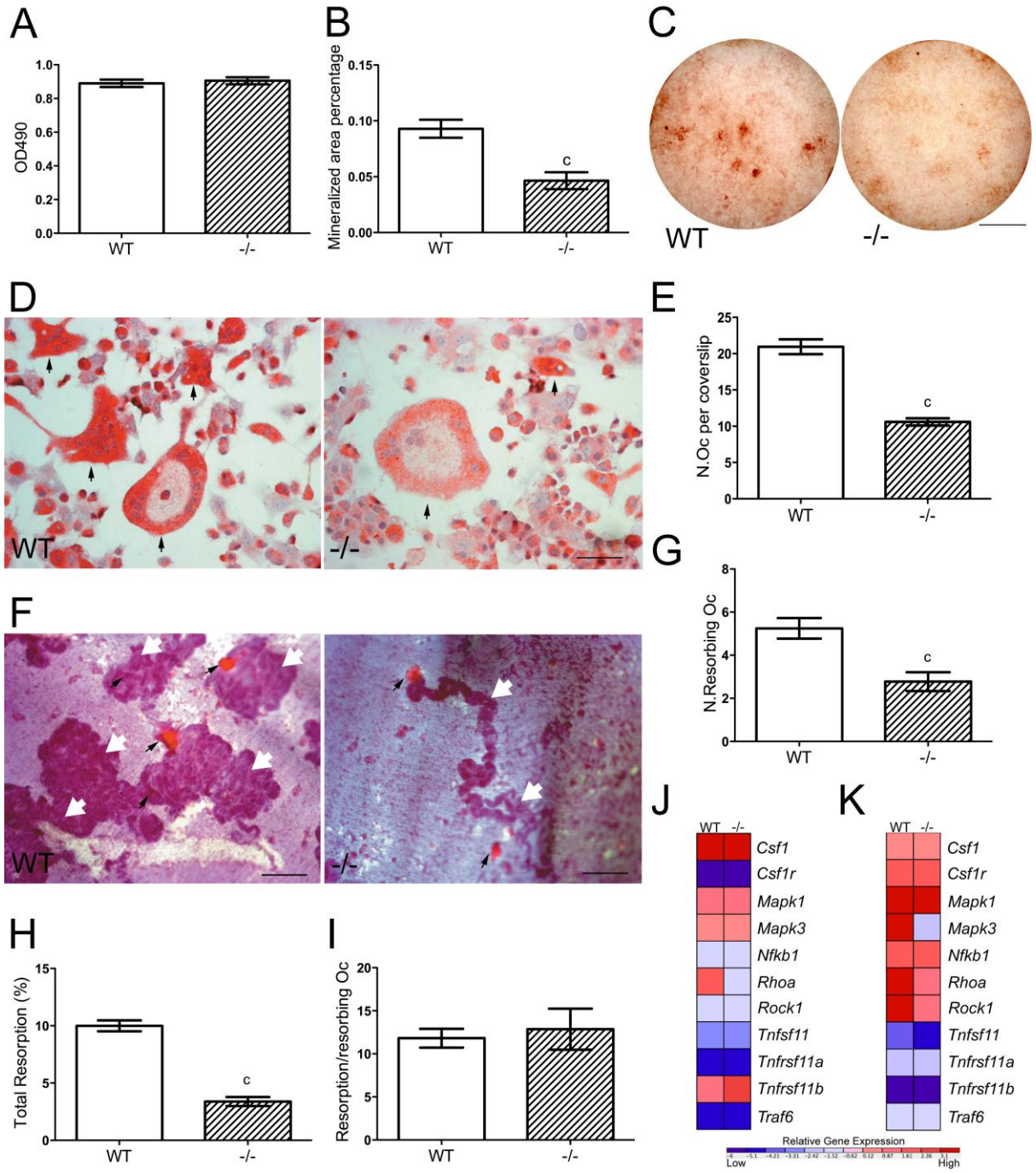

672

673

674 Figure 5

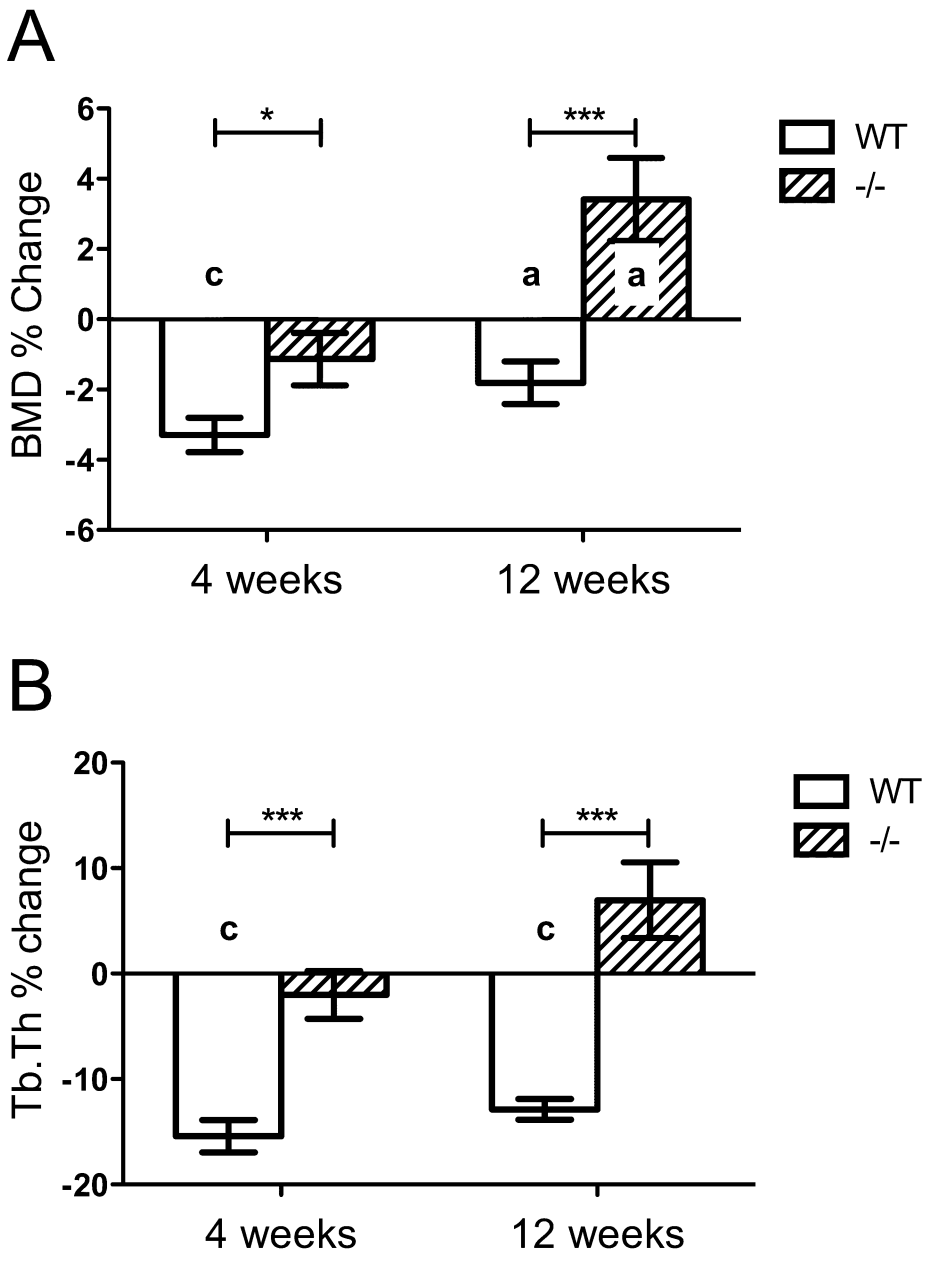

675